Properties of Hippocampal Mossy Fibre Synapses in VAMP7 KO Mice

Bernat González I Llinares, Lydia C Danglot, Thierry Galli, Christophe Mulle

European Journal of Neuroscience

WILEY

EJN European Journal of Neuroscience FENS

RESEARCH REPORT OPEN ACCESS

Properties of Hippocampal Mossy Fibre Synapses in VAMP7 KO Mice

Bernat González i Llinares[1,2] | Lydia Danglot[3] | Thierry Galli[3,4] | Christophe Mulle[1,2]

[1]Interdisciplinary Institute for Neuroscience, CNRS UMR 5297, Bordeaux, France | [2]University of Bordeaux, Bordeaux, France | [3]Institute of Psychiatry and Neuroscience of Paris, INSERM U1266, Membrane Traffic in Healthy & Diseased Brain, Université Paris Cité, Paris, France | [4]Groupe Hospitalier Universitaire (GHU) Paris Psychiatrie & Neurosciences, Paris, France

Correspondence: Christophe Mulle (christophe.mulle@u-bordeaux.fr)

Received: 29 August 2024 | **Revised:** 16 January 2025 | **Accepted:** 22 January 2025

Associate Editor: Gianmaria Maccaferri

Funding: This work was supported by the CNRS to C.M. and by the University of Bordeaux and the Erasmus Mundus program "European Neuroscience Campus" from the Seventh Framework Programme (to B.G.L.).

Keywords: hippocampus | mossy fibre synapses | presynaptic mechanisms | VAMP7 | v-SNARE

ABSTRACT

VAMP7 is a vesicular SNARE of the longin family that localizes to axons and dendrites during development, where it is important in neurite growth. In the adult brain, VAMP7 is enriched in a subset of nerve terminals, particularly in hippocampal mossy fibres (Mfs) originating from the dentate gyrus. We analysed the VAMP7 function in neurotransmitter release by detailed functional characterization of Mf synapses onto CA3 pyramidal cells in knockout mutant mice for VAMP7. We have evaluated the role of VAMP7 in different forms of short-term synaptic plasticity and the potential contribution of the co-release of glutamate and zinc. This analysis has not revealed any significant impact of the loss of VAMP7 for basal properties of synaptic transmission, for short-term plasticity, for asynchronous release and for the ability of Mf vesicles to release ionic zinc. Based on these findings, the potential role of VAMP7 in the regulation of presynaptic mechanisms is discussed.

1 | Introduction

At chemical synapses, neurotransmitter release relies on synaptic vesicle (SV) exocytosis. This process is mediated, like all other intracellular membrane fusion events, by SNAREs (for "soluble *N*-ethylmaleimide-sensitive factor attachment protein receptors") present in vesicles (v-SNAREs) and the target membrane (t-SNAREs) (also called R- and Q-SNAREs respectively, according to the conserved arginine or glutamine residue) (Weber et al. 1998). SNAREs are small (14–40 kDa) membrane-bound proteins that contain the 60–70 amino-acid α–helical coiled-coil domain called the SNARE motif (Jahn and Scheller 2006). The interaction between opposed v- and t-SNAREs impels the formation of a trans-SNARE complex, or SNAREpin, in which four SNARE motifs zipper into a four-helix bundle that brings the membranes together and ultimately catalyses their fusion (Söllner et al. 1993; Weber et al. 1998). The human genome encodes 38 SNAREs, with numerous members in each subfamily, which results in a large array of possible combinations (Gordon et al. 2010). Particular SNARE collections reside predominantly in specific subcellular compartments, where they are specialized for individual intracellular fusion reactions (Jahn and Scheller 2006). However, there are redundancies in fusion pathways, such as a SNARE complex which functions at multiple compartments, or several SNARE complexes mediating the same membrane fusion.

Abbreviations: EPSC, Excitatory Postsynaptic Current; mEPSC, miniature Excitatory Postsynaptic Current; Mf, Mossy fibre; SNAREs, soluble N-ethylmaleimide-sensitive factor attachment protein receptors; SV, synaptic vesicle (SV).

v-SNAREs are classified into the following subfamilies: the "Longins", which contain the N-terminal Longin domain (LD) extension of ~120 residues, and the "brevins", which are shorter (Filippini et al. 2001). The main SV SNARE is the brevin synaptobrevin2/VAMP2 (for "vesicle-associated membrane protein" 2). Its canonical partners at the plasma membrane are syntaxin1 and SNAP-25. In the absence of VAMP2, evoked and spontaneous neurotransmission are reduced to around 1% and 10% of control, respectively (Schoch et al. 2001). In normal physiological conditions, two VAMP2 molecules are sufficient for SV exocytosis (Sinha et al. 2011). A prototypic SV contains ~70 VAMP2 copies, but also lower levels of noncanonical v-SNAREs such as Vti1a, VAMP4, and VAMP7 (Takamori et al. 2006; Wilhelm et al. 2014). The expression of these alternative v-SNAREs probably explains the residual synaptic transmission in VAMP2 KO mice. Whether low levels of these v-SNAREs play a role in SV exocytosis in the presence of VAMP2 remains debated. The existence of SV populations expressing different v-SNAREs, or at different ratios, has been proposed to account for distinct forms of SV exocytosis (for review see (Ramirez and Kavalali 2012)). However, others claim a unique origin for SVs, independently of whether their mode of release is evoked or spontaneous (for review see (Kaeser and Regehr 2014)).

VAMP7 is a Longin v-SNARE that was first shown to associate with SNAP-23, and syntaxin3 in clostridial neurotoxin-resistant exocytotic processes at the apical plasma membrane of epithelial cells (Galli et al. 1998). VAMP7 has been reported to mediate lysosomal and granule exocytosis in several cell types (Chaineau, Danglot, and Galli 2009) including neurons (Burgo et al. 2012). Depending on the cell type, VAMP7 can interact with several t-SNAREs (syntaxin1, 3, 4, 6, 7, 8 and 10; SNAP-23, -25, -29 and -47; and Vti1b), but neither with syntaxin 13, nor 16 (for review see Rossi et al. 2004). VAMP7 is the SNARE of secretory lysosomes contributing to ATP secretion from astrocytes (Verderio et al. 2012), and to zinc secretion from HeLa cells (Kukic, Kelleher, and Kiselyov 2014). Accordingly, recent studies showed that VAMP7 mediates unconventional secretion by late endosomes of proteins of the endoplasmic reticulum like RTN3 (Wojnacki et al. 2020), the propeptide of VGF (Filippini et al. 2023) and peroxidated lipids and iron (Ralhan et al. 2023). VAMP7 also plays an important role at different steps of autophagy (for a review see (Vats and Galli 2022)). Furthermore, VAMP7 localizes to axons and dendrites during development (Coco et al. 1999), where it is important in neurite growth in cultured neurons and PC12 cells (Gupton and Gertler 2010; Racchetti et al. 2010; Alberts et al. 2003; Wojnacki et al. 2020). In the adult brain, VAMP7 is enriched in a subset of nerve terminals, particularly in mossy fibres (Mfs), the axons originating from dentate gyrus granule cells, as indicated by strong labelling in the projecting region (the stratum lucidum) in CA3 (Muzerelle et al. 2003).

The LD of VAMP7 targets the protein to presynaptic nerve terminals by binding to the δ-subunit of the clathrin-coat AP-3 (AP3δ) (Scheuber et al. 2006). In *mocha* mice, which lack AP3δ, nerve terminals are devoid of VAMP7 and the zinc-transporter ZnT3—among other cargos; and the SV and RRP size has been reported to be increased (Newell-Litwa et al. 2010; Danglot and Galli 2007).

We have previously shown using mocha mice, which are deficient in functional AP-3, that VAMP7 is lost in mocha hippocampal mossy fibre terminals, whereas the localization of VAMP 2 is unaffected (Scheuber et al. 2006). The lack of AP-3 results in increased constitutive secretion and loss of an asynchronously evoked release component. We thus wondered whether or not VAMP7 plays a role in presynaptic release using VAMP7 knock-out mice (Danglot et al. 2012). We investigated presynaptic mechanisms by characterizing synaptic transmission at hippocampal mossy fibre synapses onto CA3 pyramidal cells (Mf-CA3 synapses) which display remarkable forms of presynaptic short-term plasticity (Marneffe et al. 2024) and where VAMP7 is highly enriched presynaptically.

2 | Materials and Methods

All experiments were performed in accordance with the European Communities Council Directive of 24 November 1986 and the European Directive 2010/63/EU on the Protection of Animals used for Scientific Purposes.

2.1 | Animal Procedures and Genetically Modified Mice

VAMP7 knockout (KO) mice were generated as described in Danglot et al. 2012. The VAMP7 KO mouse line was established at the Institut Clinique de la Souris (ICS; Illkirch, France; http://www.ics-mci.fr/). The VAMP7 corresponding gene is carried on the X chromosome. Wild-type males are thus X+/Y+ while VAMP7 KO males are X−/Y+. Mice were bred at the CNRS central animal facility «CDTA Orléans» where they were constantly backcrossed on a C57BL6/N background. Wild-type males and VAMP7 KO offspring were obtained by crossing an heterozygous female with a KO male, leading to 50%–50% of wild-type and KO new born mice. Mice were housed in a temperature—and humidity-controlled animal colony on a 12 h dark–light cycle with food and water available ad libitum.

Cohorts of littermates for electrophysiology were produced at the CDTA and then sent to the Mulle lab for direct experimentation. Evaluation of VAMP7 KO efficiency was performed in Danglot et al. 2012, by PCR, western blot and immunoprecipitation to rule out any trace of proteins. Since then, mice were genotyped by PCR, and checked for absence of proteins by immunofluorescence using the 158.2 mAb against VAMP7 protein (as shown in Figure 1A).

2.2 | Slice Electrophysiology

Parasagittal hippocampal slices (320 μm) were obtained from 18- to 25-day-old male VAMP7 KO mice and WT littermates. Slices were transferred to a recording chamber in which they were continuously superfused with an oxygenated extracellular medium (95% O2 and 5% CO2) containing 125 mM NaCl, 2.5 mM KCl, 2.3 mM $CaCl_2$, 1.3 mM $MgCl_2$, 1.25 mM NaH_2PO_4, 26 mM $NaHCO_3$, and 20 mM glucose (pH 7.4). Bicuculline (10 μM) was present in the superfusate of all experiments. Whole-cell voltage-clamp recordings were made at room temperature (except for NMDA EPSCs and mEPSCs, which were made at ~32°C) from CA3 pyramidal cells under infrared differential interference contrast imaging with

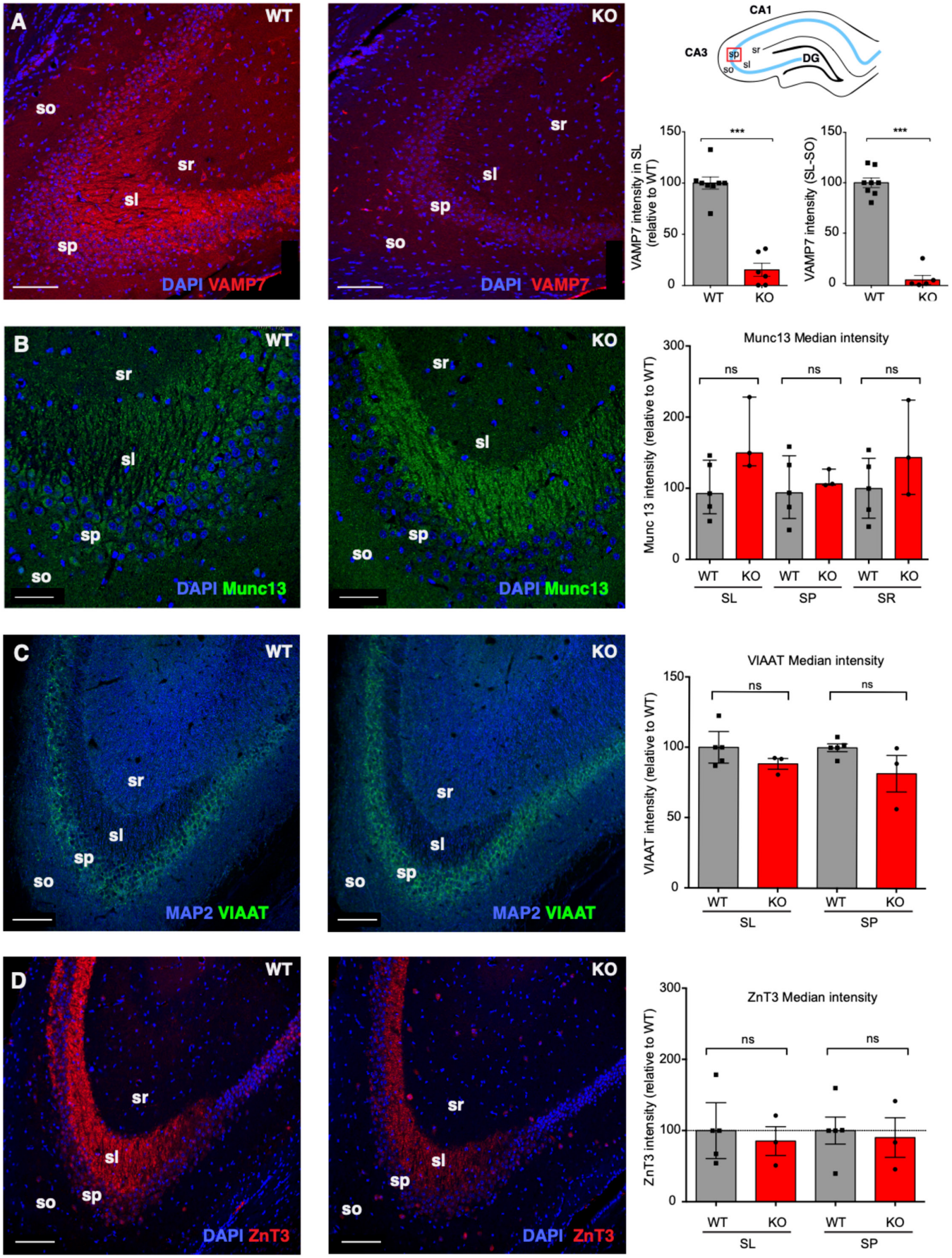

FIGURE 1 | Legend on next page.

FIGURE 1 | Sagittal sections of WT and VAMP7 KO hippocampus stained with DAPI plus VAMP7, Munc13, VIAAT and ZnT3. (A) VAMP7 immunolabelling is lost in VAMP7 KO mice. Scale bar = 300 μm. Quantification of immunofluorescence signal in the stratum lucidum shown in the right panels ($n = 8$ WT and $n = 6$ VAMP7 KO mice). (B) Munc13–1 expression in VAMP KO mice. Scale bar = 100 μm. Quantification of immunofluorescence signal in the stratum pyramidale, stratum lucidum and stratum radiatum shown in the right panels ($n = 5$ WT and $n = 3$ VAMP7 KO mice). (C) VIAAT expression. Quantification of immunofluorescence signal in the stratum pyramidale and stratum shown in the right panels (n = 5 WT and n = 3 VAMP7 KO mice). Scale bar = 100 μm. (D) ZnT3 expression. Quantification of immunofluorescence signal in the stratum pyramidale and stratum shown in the right panels ($n = 5$ WT and $n = 3$ VAMP7 KO mice). Scale bar = 100 μm. CA1/CA3: Cornus Ammonis 1 and 3, sr: stratum radiatum, sluc: stratum lucidum, sp: stratum pyramidale, so: stratum oriens. Data from $n = 5$ WT and $n = 3$ VAMP7 KO mice.

borosilicate glass capillaries, which had resistances between 4 and 8 MΩ. For AMPA EPSCs the patch electrodes were filled with a solution containing 140 mM $CsCH_3SO_3$, 2 mM $MgCl_2$, 4 mM NaCl, 5 mM phospho-creatine, 2 mM Na_2ATP, 0.2 mM EGTA, 10 mM HEPES, and 0.33 mM GTP (pH 7.3) adjusted with CsOH. For NMDA EPSCs the patch electrodes were filled with a solution containing (in mM): 120 caesium methanesulfonate, 2 $MgCl_2$, 4 NaCl, 5 phospho-creatine, 2 Na_2ATP, 20 BAPTA, 10 HEPES, 0.33 GTP (pH 7.3) adjusted with CsOH.

MF-CA3 EPSCs were evoked by minimal intensity stimulation (Marchal and Mulle 2004) via a glass electrode (about 1 μm tip diameter) positioned in the hilus region of the dentate gyrus. Stimulation pipettes were filled with 1 M NaCl and stimulation pulses in basal conditions were provided at 0.1 Hz (200 ms duration, 5–40 V and 15–30 mA amplitude). MF synaptic currents were identified according to the following criteria: robust low frequency facilitation, low release probability at 0.1 Hz, rapid single rise times (~1 ms), and decays free of secondary peaks that may indicate the presence of polysynaptic contamination.

The access resistance was < 20 MΩ and recordings were discarded if it changed by > 20%. No series resistance compensation was used. Recordings were made using an EPC 9.0 or EPC 10.0 amplifier, which were run with Pulse and Patch Master software (HEKA Elektronik, Lambrecht/Pfalz, Germany), respectively. Data were filtered at 3 kHz, digitized at 10 or 20 kHz, and stored on a personal computer for additional analysis. Basal synaptic responses were evoked every 10 s (0.1 Hz).

To record NMDA EPSCs, cells were voltage-clamped at +40 mV and NMDA EPSCs isolated by blocking AMPA and kainate receptors with 20 μM NBQX. The selective $GABA_B$ receptor antagonist CGP 55845 was also added at 3 μM to better record responses to trains of stimuli. To record mEPSCs, 0.5 μM TTX was added to the extracellular medium. Bicuculline methochloride, 2,3-dihydroxy-6-nitro-7-sulfamoyl-benzo[f]quinoxaline-2,3-dione (NBQX), D-(−)-2-amino-5-phosphonovaleric acid (D-APV), CGP 55845, and TTX were from Tocris. All other compounds were from Sigma-Aldrich.

2.3 | Data Analysis and Statistics

Data were analysed using IGOR Pro (Wavemetrics, Lake Oswego, OR). Results are expressed as mean ± SEM, unless otherwise indicated; *n* indicates the number of different cells. Statistical comparisons were performed using Student's *t* test and statistical significance was set at 0.05. Statistical comparison between normalized data was performed using nonparametric Mann–Whitney test. EPSC amplitudes during trains of stimulation were obtained by measuring the maximal amplitude value reached during the train of EPSCs. Statistical analysis was performed with GraphPad Prism software.

2.4 | Immunohistochemistry

Mice (5 WT and 3 KO) were anaesthetised with pentobarbital (60 mg/kg, ip) then intracardially perfused with 4% paraformaldehyde (PFA) in PBS. Tissues were postfixed for 1 h in 4% PFA and cryoprotected in PBS-sucrose 30% (w/v) overnight. Cryotome sections (50 μm) were incubated in PBS-NH_4Cl (20 min, room temperature) and permeabilized in PBS + 0.1% Triton, 0.2% gelatin (PBSTg). Sections were then incubated for 2 days at 4°C with the primary antibodies in PBSTg and with the secondary antibodies for 3 h. Controls without primary antibody were always negative. Specimens were observed with a 20× oil immersion objective, followed by a 1.1 digital zoom magnification. Images were acquired on a Leica SP5 or SP8 confocal microscope by sequential scanning of the emission lines. Alexa 488 was detected by using the 488 nm-line of an argon laser for excitation; Cy3 and Cy5 were respectively excited by the 543 nm-line of a green neon laser and the 650 nm-line of a helium neon laser. Typically, sections (4096 × 4096 pixels), with an interval of 0.32 μm, were scanned three times, to optimize the signal/noise ratio. Quantifications were performed using ICY software.

The antibodies used were: mAb anti TI-VAMP/VAMP7 (clone158.2 Synaptic systems), rabbit polyclonal anti-Munc13-1 (Synaptic Systems), mouse monoclonal anti-ZnT3 (Synaptic Systems), and rabbit polyclonal anti-VIAAT (1:500 provided by Bruno Gasnier, Paris).

3 | Results

3.1 | The Expression of Presynaptic Proteins in the Stratum Lucidum is not Significantly Affected in VAMP7 KO Mice

VAMP7 is highly expressed in the hippocampal mossy fibre (Mf) track originating from dentate gyrus granule cells (Figure 1A). We have quantified VAMP7 immunolabelling within the stratum lucidum (sl), the region where Mfs make synaptic contacts onto CA3 cells. The fluorescence signal was decreased by 85% ± 6.8% in VAMP7 KO vs. WT mice (Figure 1A) (average data from $n = 8$ WT mice and $n = 6$ VAMP7 KO mice). The remaining signal in VAMP7 KO mice is likely due to non-specific binding of antibodies to Fc receptors in the absence of target. We

performed a second quantification of labelling intensity within the stratum lucidum by subtracting background fluorescence signal using the stratum oriens as a control region. This indicated a nearly total loss (decrease by 96.5% ± 4.5%) of immunolabelling for VAMP7 further suggesting that the KO was indeed fully effective. We tested whether the loss of presynaptic VAMP7 impacts the expression of canonical presynaptic proteins in the sl. We used immunolabelling for several presynaptic proteins, and expression intensity in VAMP7 KO mice was normalized to the average WT expression. The Munc13-1 protein was used as a canonical presynaptic marker (Figure 1B). Munc-13-1 intensity was not changed significantly increased in stratum lucidum (100 ± 17.4 vs. 169.8 ± 29.7 respectively, p value = 0.1429), stratum pyramidale (100 ± 20.8 vs. 112.5 ± 7.2, respectively, p value = 0.7857) and stratum radiatum (100 ± 19.5 vs. 152.9 ± 38.6, respectively, p value = 0.3929). To rule out a potential general effect on excitatory and inhibitory synapses, we proceeded to the labelling of GABAergic presynaptic boutons with a VIAAT (Vesicular Inhibitory Amino Acid Transporter) staining, but we did not notice any obvious difference (Figure 1C). Because VAMP7 targeting in presynaptic terminals is dependent on the molecular adaptor AP3, we also checked the expression of the zinc transporter ZnT3, a presynaptic vesicular molecule whose targeting is also AP3-dependent (Newell-Litwa et al. 2010). In VAMP7 KO mice, ZnT3 intensity (Figure 1D) was not changed significantly in stratum lucidum (100 ± 21.6 vs. 85.3 ± 20.2,

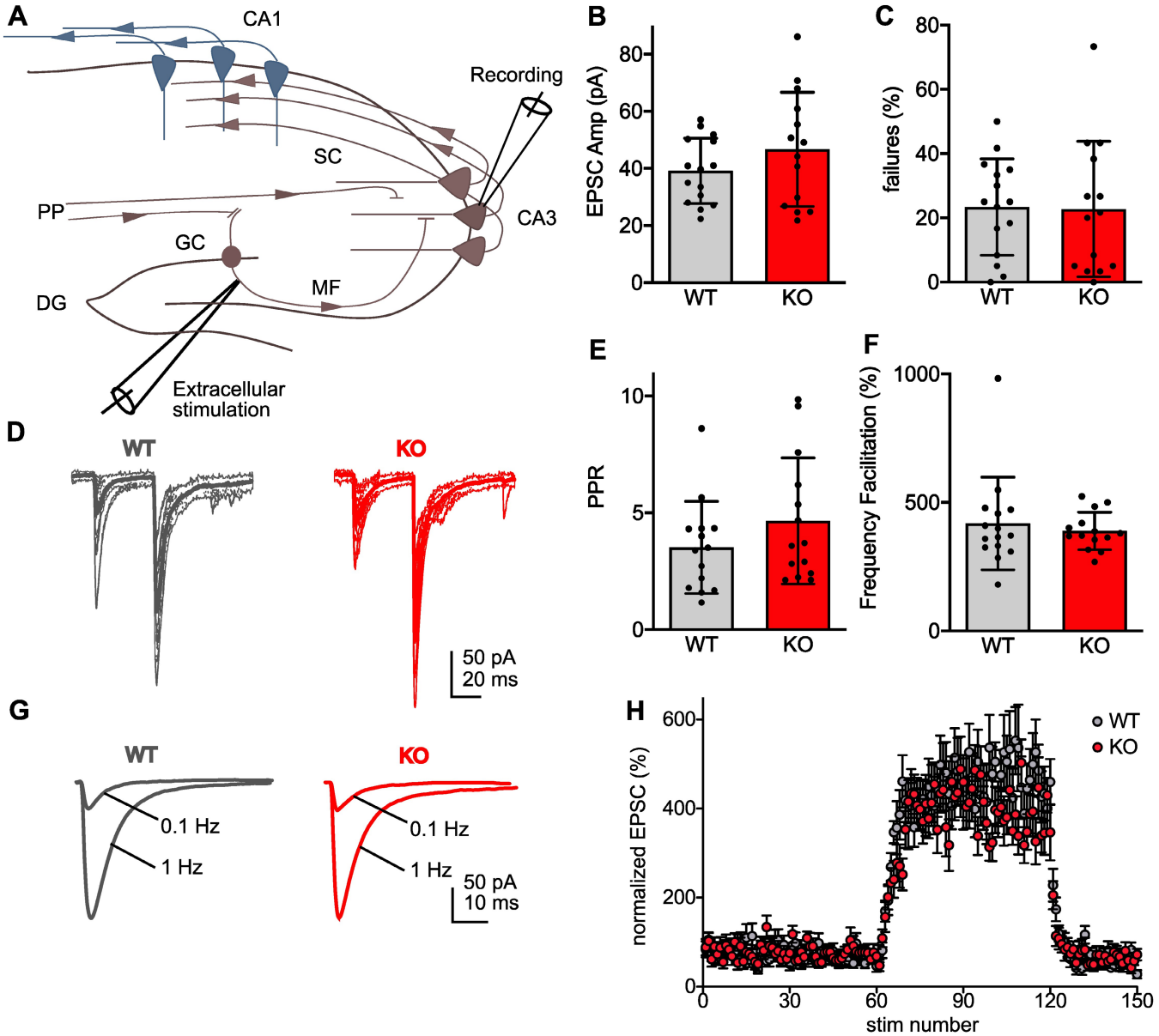

FIGURE 2 | Basal evoked transmission and short-term plasticity are unaltered in VAMP7 KO. (A) Schematic diagram of a hippocampal slice displaying the recording (right, in a CA3 pyramidal cell) and stimulating electrodes (left, inside the dentate gyrus). (B)–(C) Comparison for average basal EPSC amplitudes and percentage of failures. (D) Sample traces evoked by two stimuli with a 40 ms inter-stimulus interval and over-imposed average. (E)–(F) Comparison for Paired Pulse Ratio (PPR) and Frequency Facilitation (FF). (G) Sample average traces evoked at 0.1 and 1 Hz. H, Time course of FF, EPSCs were normalized to the mean amplitude of the 10 min baseline at 0.1 Hz (60 stimuli) preceding the stimulation increase to 1 Hz (60–120th stimuli), and final 30 stimuli at 0.1 Hz. Results from $n = 15$ WT and $n = 14$ VAMP7 KO CA3 PCs, from n = 8 WT and $n = 9$ VAMP7 KO mice. The error bars represent ±S.E.M.

respectively, p value = 0.7321) and stratum pyramidale (100 ± 19 vs. 90.3 ± 27.9, respectively, p value = 0.7143), indicating that ZnT3 is still able to reach the presynaptic Mf boutons in the absence of the VAMP7 vSNARE on the AP3 vesicles.

3.2 | Basal Transmission and Short-Term Plasticity are not Impaired in VAMP7 KO Mice

We tested the potential role of VAMP7 in controlling neurotransmitter release and plasticity at Mf-CA3 synapses. We recorded CA3 pyramidal cells in the whole-cell voltage clamp mode in slices from WT and VAMP7 KO mice, and we evoked Mf-EPSCs by minimal stimulation of Mfs with an electrode positioned in the DG (Marchal and Mulle 2004) (Figure 2A). The average amplitude of Mf-EPSCs evoked at a frequency of 0.1 Hz was not significantly different between the two genotypes (WT: 46.7 ± 5.3 pA, n = 14; VAMP7 ko 39.2 ± 2.9 pA, n = 15; p value = 0.2184) (Figure 2B). The rate of failure of Mf-EPSCs, which is indicative of the initial release probability at Mf-CA3 release sites, was similar in WT and VAMP7 ko mice (22.7 ± 5.6% and 23.3 ± 3.9%, respectively) (Figure 2C). These results indicate that the basal properties of Mf-CA3 synapses are not affected by the loss of VAMP7.

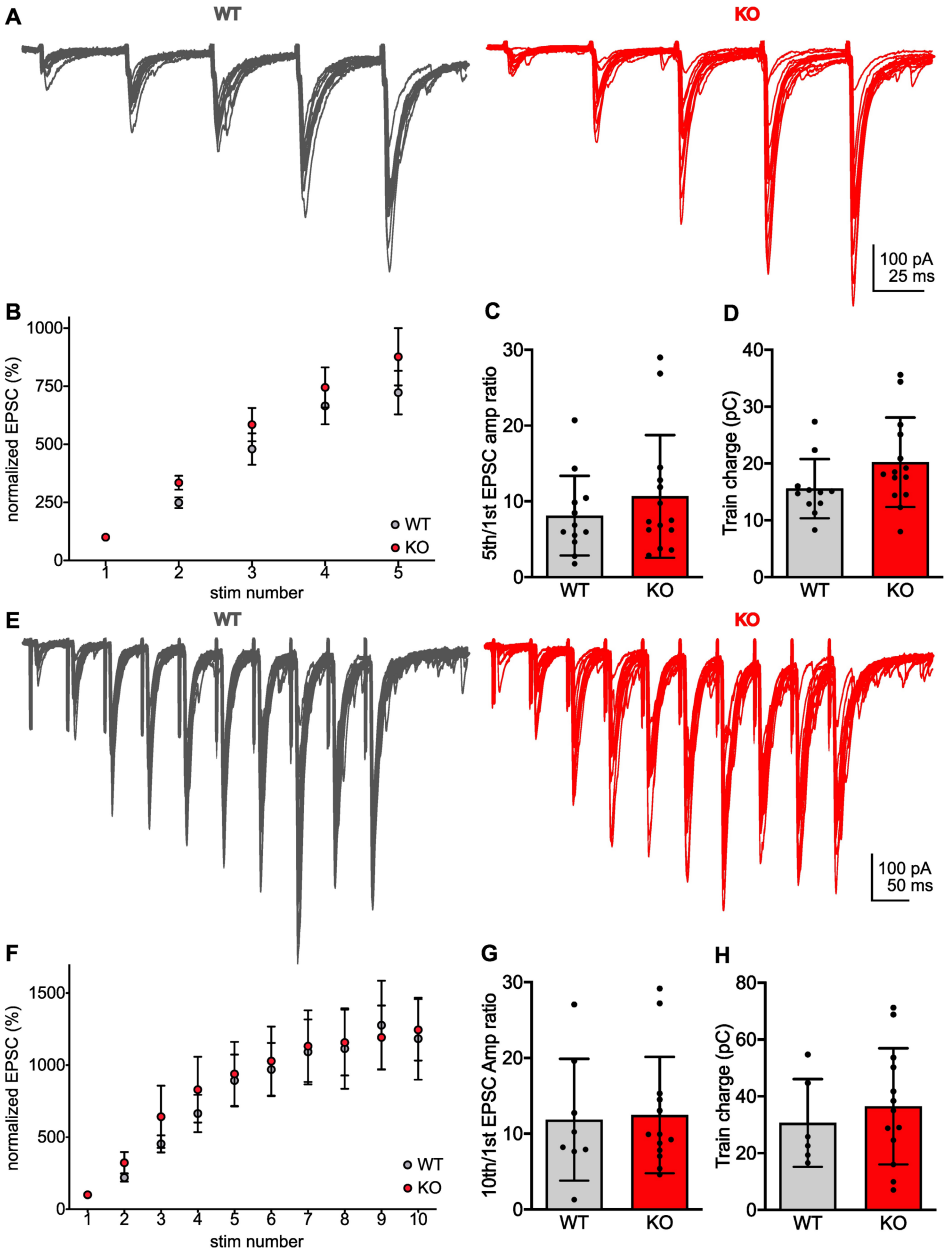

FIGURE 3 | Short-term synaptic plasticity evoked by short bursts is not affected in the absence of VAMP7. (A) Sample traces evoked by five stimuli at 20 Hz and over-imposed average. (B) EPSC facilitation as normalized to the average amplitude of the first stimulus (n = 11 WT and n = 14 VAMP7 KO mice). (C)–(D) Comparison of the average EPSC amplitude of the first stimulus, and average train charge. (E) Sample traces evoked by 10 stimuli at 20 Hz and over-imposed average (n = 8 WT and n = 13 VAMP7 KO CA3 PCs from n = 5 WT and n = 9 VAMP7 KO mice). (F) EPSC facilitation as normalized to the average amplitude of the first stimulus. (G)–(H) Comparison of the average EPSC amplitude of the first stimulus, and average train charge. The error bars represent ±S.E.M.

We then examined whether different forms of short-term plasticity were altered in VAMP7 KO mice. Differences in the extent of paired-pulse facilitation, consisting in two stimulations separated by a short time interval (e.g. 40 ms), is generally used to test for changes in release probability. Paired-pulse ratio (PPR) was not changed significantly in VAMP7 ko mice (4.7 ± 0.7 in VAMP7 KO vs. 3.5 ± 0.5 in WT, p value = 0.2155) (Figure 2D,E). Mf-CA3 synapses undergo a rather unique form of presynaptic plasticity named frequency facilitation (FF) (see Rebola, Carta, and Mulle 2017). FF corresponds to the marked facilitation of Mf-CA3 synaptic transmission upon increasing the steady rate of stimulation from low (0.1 Hz) to moderate (from 0.5 to 3 Hz). FF was not significantly altered in VAMP7 ko mice (WT: 388 ± 19% n = 14; VAMP7 ko, 418 ± 47%, n = 13; Student's unpaired t test, p value = 0.5782) (Figure 2F–H). We also tested train facilitation by stimulating Mfs with either five or 10 stimuli at 20 Hz (Figure 3). Mf-CA3 EPSC facilitation, as normalized to the average amplitude of the first stimulus, was not affected for neither train stimuli number (Figure 3B,C,F,G) (Student's unpaired t test, p value = 0.2087 and 0.175, respectively). Finally, the total charge for each train (20.2 ± 2.1 pC in VAMP7 KO vs. 15.6 ± 1.6 pC in WT for five stimuli, and 36.5 ± 5.7 pC in VAMP 7 ko vs. 30.6 ± 6.3 pC in WT for 10 stimuli) was not statistically significant (Student's unpaired t test, p value = 0.1062 and 0.5424, respectively) (Figure 3D,H). In keeping with the immunocytochemical labelling of Munc13 suggesting no significant change of synaptic release sites in VAMP7 ko mice, we found not difference in the amplitude or failure rate of evoked Mf-CA3 EPSC, which correlate with number of active release sites per Mf bouton.

We then tested if the loss of presynaptic VAMP7 impacted on spontaneous release activity. Neither the frequency nor the amplitude of mEPSCs were altered in VAMP7 ko mice (Figure 4). mEPSCs recorded in CA3 pyramidal cells arise from Mf synapses as well as from A/C and perforant path glutamatergic synapses. We separated synaptic events according to their amplitude, considering that Mf-CA3 EPSCs display on average higher quantal size. The frequency of large mEPSCs (> 25 pA) was not significantly different in both genotypes (0.92 ± 0.17 Hz, n = 23 in WT vs. 1.20 ± 0.19, n = 23 in VAMP7 KO). It thus appeared that evoked and spontaneous EPSCs are not significantly altered in VAMP7 KO mice.

3.3 | Plasticity of Evoked Mf-EPSCs After Long Bursts is not Altered in VAMP7 KO Mice

ZnT3-containing (Lavoie et al. 2011) and VAMP7-containing (Hua et al. 2011) synaptic vesicles represent a pool of vesicles which appear to be released more reluctantly. We thus reasoned that synaptic release events evoked after long trains of stimulation which would unravel this reluctant pool could be impaired. We applied 5 s-trains at 10, 20, and 40 Hz (Figure 5). Similarly to shorter trains, when Mf-EPSC amplitude was normalized to the average of the first stimuli, the extent of plasticity evoked by long trains was also unaffected (Figure 5). The amplitude of the first EPSC in either of the trains were not significantly different between the two genotypes mice for 10, 20 and 40 Hz trains (10 Hz: 165 ± 39 pA vs. 123 ± 66 pA in WT; 20 Hz: 166 ± 25 pA vs. 115 ± 32 pA; 40 Hz: 129 ± 22 pA vs. 143 ± 65 pA; Student's unpaired t test, p value = 0.5652; 0.2401, and 0.8063, respectively).

3.4 | Asynchronous Release After Short and Long Bursts is not Altered in VAMP7 KO Mice

Treatment of cultured hippocampal slices with TeNT revealed an asynchronous release component in WT but not in slices of *mocha* mice, and no asynchronous release was observed in TeNT-untreated explants by stimulation at 0.1 Hz (Scheuber et al. 2006). We thus investigated asynchronous release in VAMP7 KO mice. Asynchronous Mf-EPSCs occur during several hundreds of ms following prolonged bursts of stimulation (Figure 6). We calculated for each genotype the average number of asynchronous events and median amplitude (per bins of 10 ms), in the 500 ms preceding and following short bursts (i.e. trains of five at 20 Hz) (Figure 6A). Next, we compared the frequency of events in the 100 ms post-stimulation to the frequency of the events in the 500 ms baseline prior to the train of stimuli

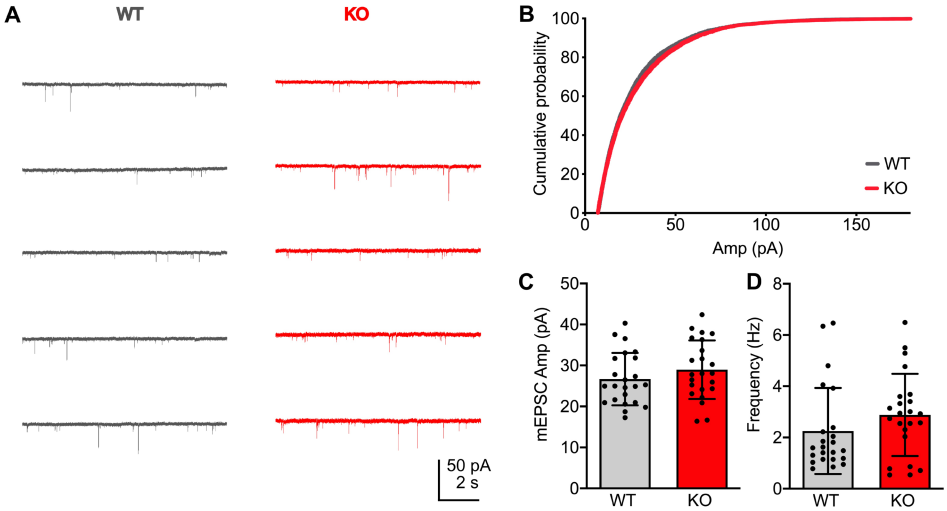

FIGURE 4 | Spontaneous synaptic release is unaltered in VAMP7 KO mice. (A) Sample traces of mEPSC recordings in WT and VAMP7 KO mice. (B) Cumulative probability plot for the first 300 events. (C)–(D) Comparison of the average amplitude and frequency of mEPSCs. N = 23 WT and n = 23 VAMP7 KO CA3 PCs, from n = 3 WT and n = 4 VAMP7 KO mice. The error bars represent ±S.E.M.

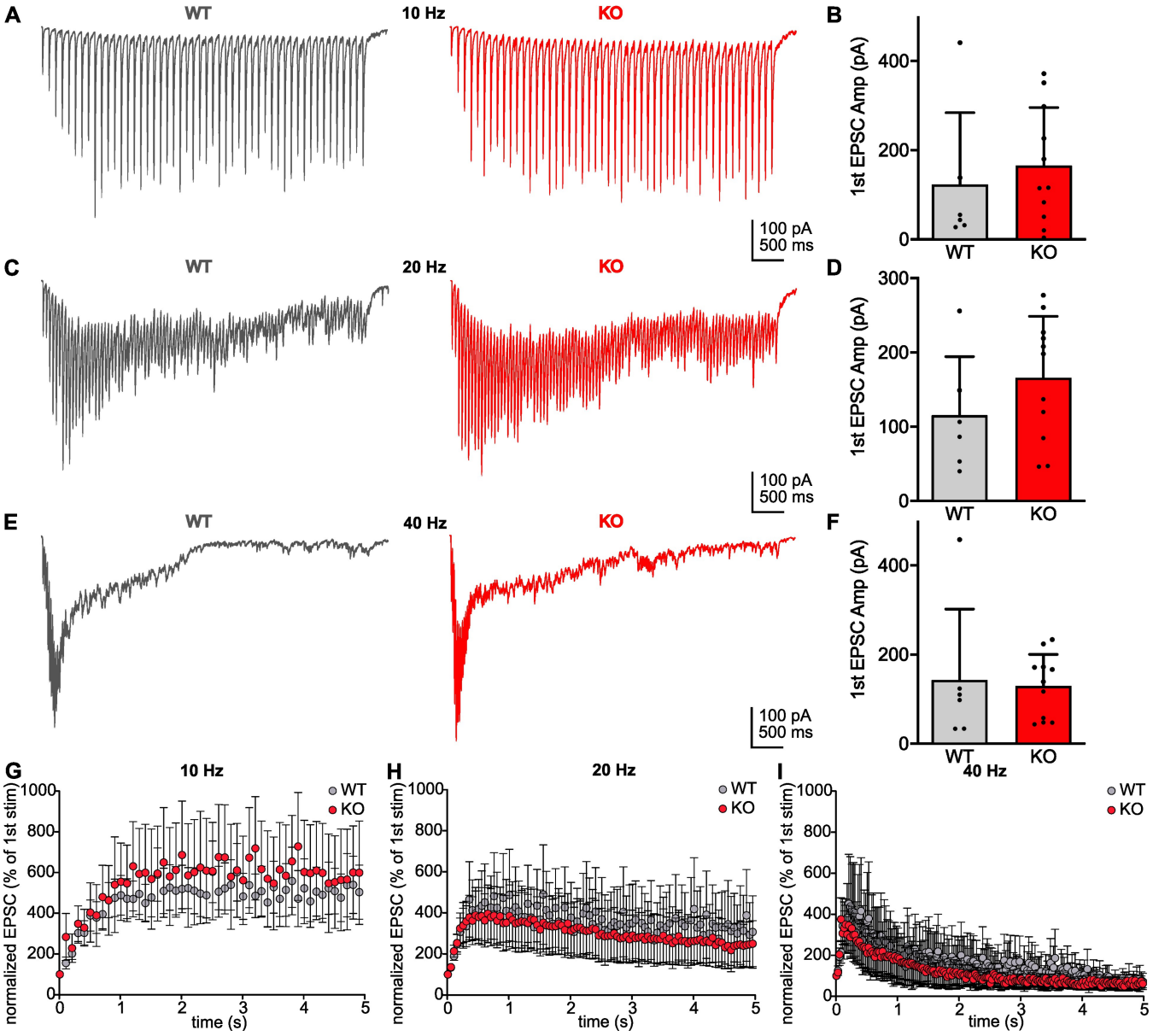

FIGURE 5 | Evoked plasticity by long bursts is not affected in the absence of VAMP7. (A) Sample traces of average EPSCs evoked by 5 s-trains at 10 Hz. (B) Comparison of the average EPSC amplitude of the first stimulus at 10 Hz. (C) Sample traces of average EPSCs evoked by 5 s-trains at 20 Hz. (D) Comparison of the average EPSC amplitude of the first stimulus at 20 Hz. (E) Sample traces of average EPSCs evoked by 5 s-trains at 40 Hz. (B) Comparison of the average EPSC amplitude of the first stimulus at 40 Hz. (G)–(I) EPSC facilitation as normalized to the average amplitude of the first stimulus for 5 s-trains at 10, 20, and 40 Hz, respectively. $N = 6$ WT and $n = 11$ VAMP7 KO CA3 PCs, from $n = 5$ WT and $n = 6$ VAMP7 KO mice. The error bars represent ±S.E.M.

(Figure 6B). The ratio of frequencies (post vs. pre) did not differ in the absence of VAMP7 after five stimuli (18.2 ± 5.3 vs. 17.7 ± 6.5 in WT, p value = 0.9561). We also compared the cumulative probability of the asynchronous events (Figure 6C), without finding any disparity (Kolmogorov–Smirnov test, p value = 0.1798). Finally, we compared the average median amplitude of the preceding 500 ms ('pre'), the 100 ms post-stimulation ('10 bins post') and the 500 ms post-stimulation ('post') (Figure 6D). One-way ANOVA tables for these multiple comparisons are shown as supplementary material (Supplementary Table S1).

We then examined whether asynchronous release following long bursts of stimulation was altered in the absence of VAMP7. Long bursts (namely trains of 5 s at 10, 20, and 40 Hz) (Figure 7) give rise to numerous and complex EPSCs that follow bursts of stimulation for up to 500 ms. Thus, instead of counting the number of events, we chose to compare the charges of the first 500 ms of each train, the total train charge (5 s), and the subsequent 500 ms of asynchronous release (Figure 7G,H,I, respectively). The initial charge (first 500 ms) increased linearly with increasing stimulation frequency, and despite a higher charge at all frequencies in KO slices, this tendency did not reach statistical significance (Figure 7G and supplementary Table S2). On the other hand, the total train charge and asynchronous charge attained a maximum at 20 Hz, and decreased at 40 Hz, while no significant difference

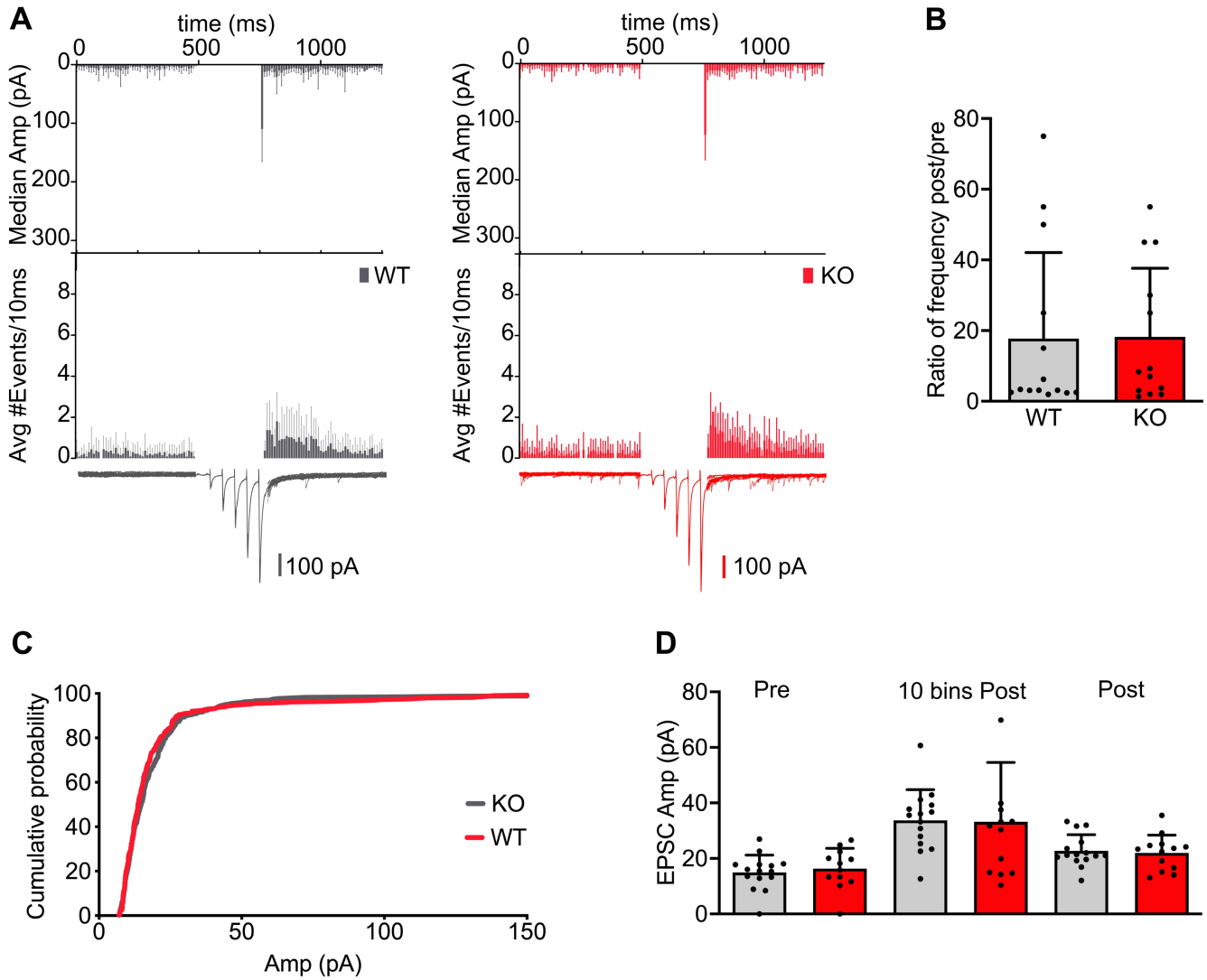

FIGURE 6 | Asynchronous release after short bursts is not affected in the absence of VAMP7. (A) From top to bottom, median amplitude and average number of events per 10 ms bins, displayed over sample traces of average EPSCs evoked by trains of five stimuli, flanked by overlaid sample traces of baseline and asynchronous events. (B) Comparison of the frequency of events in the 100 ms post-stimulation as ratio of the events during the preceding 500 ms. (C) Cumulative probability plot for the asynchronous events. (D) Comparison of the average median amplitudes of the events in:the preceding 500 ms, the 100 ms post-stimulation, and 500 ms post-stimulation, for trains of five. $N = 8$ WT and $n = 13$ VAMP7 KO CA3 PCs, from $n = 7$ WT and $n = 9$ VAMP7 KO mice. The error bars represent ±S.E.M.

was observed between genotypes (Figure 7H,I) (supplementary Tables S3 and S4, respectively). Overall our comparison did not reveal any significant differences in the ability of Mf-CA3 synapses to evoke asynchronous release in the absence of VAMP7.

3.5 | Synaptic Release of Zinc in the Absence of VAMP7

The targeting of the zinc transporter ZnT3 depends on the molecular adaptor AP3 as for VAMP7. This suggests that VAMP7 is expressed in zinc containing vesicles. Although the expression of ZnT3 is only moderately decreased in VAMP7 ko mice, we tested whether zinc release from Mf terminals may be affected in the absence of VAMP7. To examine the dynamics of zinc release at excitatory synapses, in particular at Mf-CA3 synapses, we took advantage of the possibility to assess the modulation of NMDAR EPSCs by zinc through the high nanomolar sensitivity of the GluN2A NMDAR subunit for zinc at Mf-CA3 synapses (Vergnano et al. 2014). A single synaptic event is unable to produce zinc modulation of NMDA synaptic currents at this low release probability synapse, while modulation is apparent at higher release probability SC-CA1 synapses and at Mf-CA3 synapses which were conditionally shifted to higher release probability (Vergnano et al. 2014).

We recorded from NMDA-mediated EPSCs at +40 mV in the presence of NBQX to block AMPA and kainate receptors. In order to detect a modulation of NMDA-EPSCs by synaptically released zinc at Mf-CA3 synapses, we increased release probability by conditioning with 10 stimuli at 3 Hz, then applied a train of seven stimuli at 25 Hz (Figure 8). This protocol should enable to evaluate whether the amount of zinc being released at Mf-CA3 is altered in VAMP7 ko mice, by the extent of NMDA-EPSC inhibition during the train. We found no difference in the

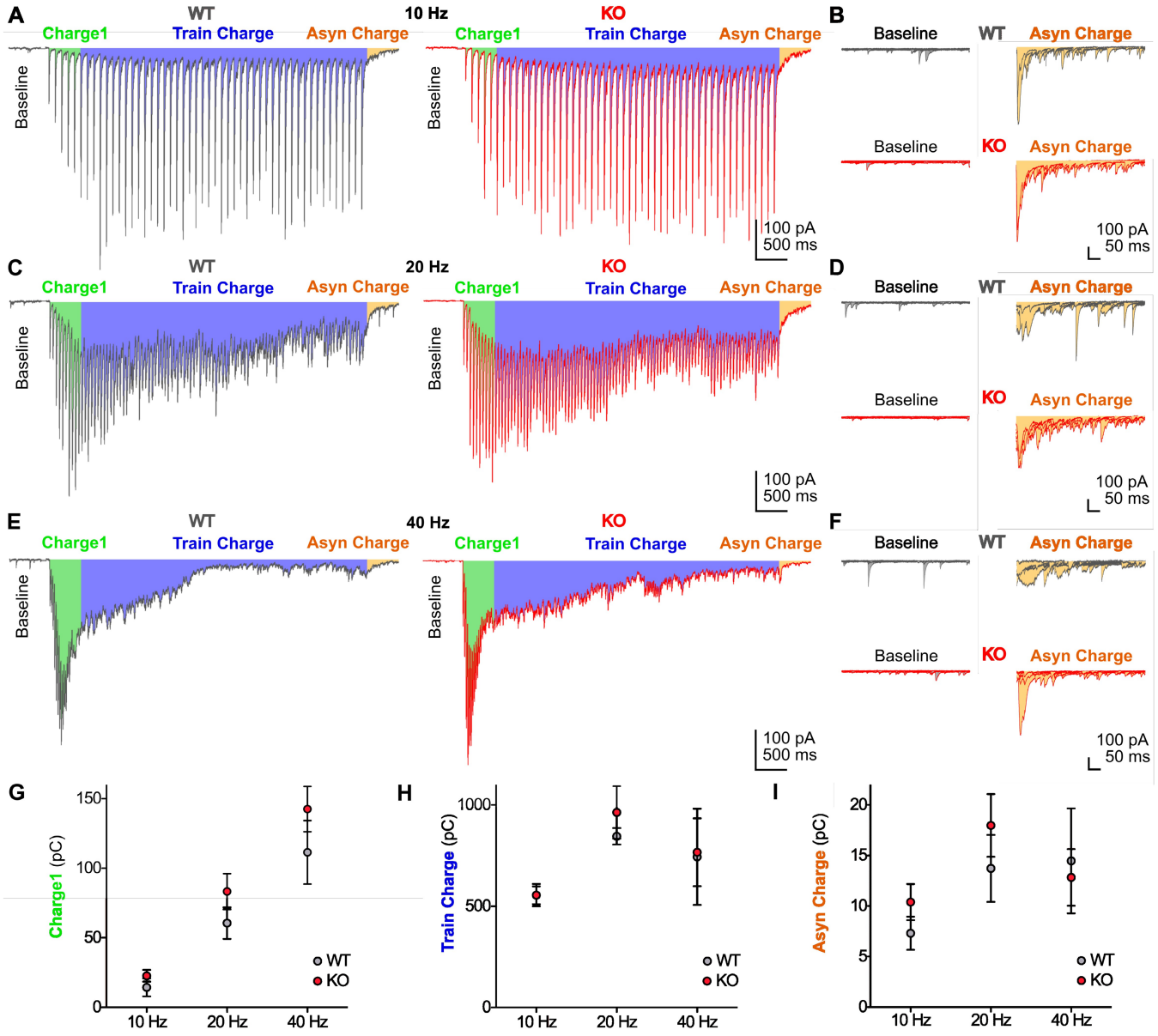

FIGURE 7 | Asynchronous release during and after long bursts is not impacted in VAMP7 KO mice. (A) Sample traces of average EPSCs evoked by 5 s-trains at 10 Hz, including the preceding 500 ms baseline, and subsequent 500 ms of asynchronous release. Charges calculated are represented by the respective coloured area (train charge includes both the blue and green areas). (B) Overlaid sample traces of 500 ms baseline and asynchronous release, with calculated area coloured in grey and orange, respectively. (C) Sample traces of average EPSCs evoked by 5 s-trains at 20 Hz, including the preceding 500 ms baseline, and subsequent 500 ms of asynchronous release. Charges calculated are represented by the respective coloured area (train charge includes both the blue and green areas). (D) Overlaid sample traces of 500 ms baseline and asynchronous release, with calculated area coloured in grey and orange, respectively. (E) Sample traces of average EPSCs evoked by 5 s-trains at 40 Hz, including the preceding 500 ms baseline, and subsequent 500 ms of asynchronous release. Charges calculated are represented by the respective coloured area (train charge includes both the blue and green areas). (F) Overlaid sample traces of 500 ms baseline and asynchronous release, with calculated area coloured in grey and orange, respectively. (G–I) Comparisons between genotypes of the different charges calculated for each frequency. $N = 6$ WT and $n = 6$ VAMP7 KO CA3 PCs from $n = 5$ WT and $n = 6$ VAMP7 KO mice. The error bars represent ±S.E.M.

NMDA-response to the train at 25 Hz between the two genotypes (Figure 8) indicating that zinc is released at comparable levels in WT and VAMP7 ko mice.

4 | Discussion

VAMP7, a synaptic v-SNARE is abundantly expressed in the hippocampal stratum lucidum, the region where Mfs make synaptic contacts with CA3 pyramidal cells and interneurons. VAMP7-containing vesicles have been shown to preferentially replenish resting pool that contributes only minimally to evoked release but may comprise a reluctantly released pool of vesicles (Hua et al. 2011). This prompted us to directly examine the consequences of the loss of VAMP7 on spontaneous and evoked synaptic transmission and plasticity at Mf-CA3 synapses. Here we found no change in Munc13 and VIAAT labelling intensity in the stratum lucidum, suggesting

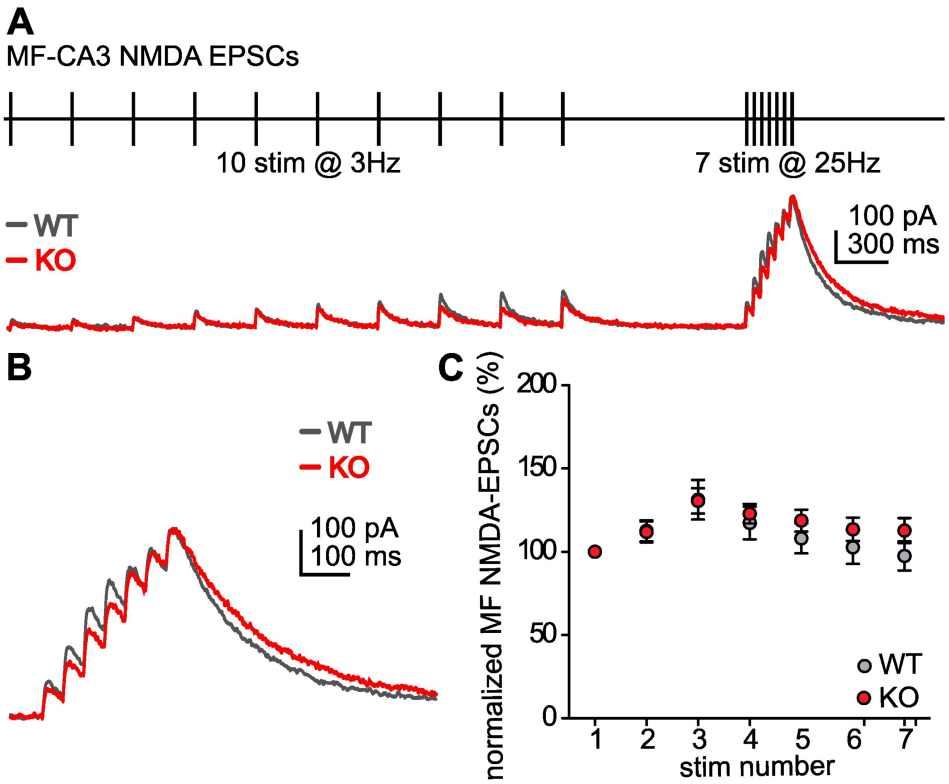

FIGURE 8 | Zinc is normally released in the absence of VAMP7. (A) The probability of release at Mf synapses was increased by applying a conditioning stimulus (10 stimulations at 3 Hz) prior to burst stimulation (seven stimuli at 25 Hz). (B) After the conditioning stimulus, burst stimulation induced similar potentiation of NMDA-EPSCs in WT and VAMP7 KO slices, which indicates similar zinc release in both genotypes. (C) Data were normalized to the amplitude of the first NMDA-EPSC in the burst and are presented as mean ± S.E.M. $N = 13$ WT and $n = 16$ VAMP7 KO CA3 PCs, from $n = 6$ WT and $n = 7$ VAMP7 KO mice.

unchanged number of synaptic release sites at Mf terminals of VAMP7 ko mice. The basic properties of evoked Mf-EPSCs were not affected, indicating no overt change in the quantal parameters and release probability at individual release sites. We found no evidence for an impairment of short-term presynaptic plasticity in response to trains of stimulation at various frequencies. Finally, monitoring NMDAR EPSCs at Mf-CA3 synapses did not reveal any deficit in the release of vesicular zinc in VAMP7 KO.

In *mocha* mice, which are deficient in functional AP-3, VAMP7 is similarly lost in hippocampal Mf terminals, whereas the localization of synaptobrevin 2 is unaffected (Scheuber et al. 2006). In these mice, evoked Mf-CA3 transmission is normal, but spontaneous miniature EPSCs (mEPSCs) release frequency increased (Scheuber et al. 2006). In contrast, we did not observe any change in the frequency of mEPSCs, and we found that the frequency and amplitude of asynchronous events, which occur in a delayed manner following long-lasting trains of stimulation were not different in the absence of presynaptic VAMP7. Interestingly, this form of synaptic release was shown to be selectively diminished in AP-3b2 KO mice (Evstratova et al. 2014). This suggests that the synaptic phenotype of mice lacking AP-3 cannot be explained by a deficient targeting of VAMP7 to Mf synaptic vesicles. The presynaptic electrophysiological defects observed at Mf-CA3 synapses in *mocha* mice are likely not solely due to the loss of presynaptic VAMP7.

VAMP7-pHluorin overexpressed in cultured neurons preferentially labels vesicles unresponsive to stimulation (Hua et al. 2011). In addition, overexpression of the LD increases the spontaneous release of VAMP7-pHluorin and VAMP2-pHluorin but not VGLUT1-pHluorin in mature neurons (Hua et al. 2011). In contrast, the LD inhibits VAMP7-pHluorin but not VAMP2-pHluorin in developing neurons (Gupton and Gertler 2010). In the presence of bafilomycin, TeNT essentially abolishes the response of VGLUT1 to 10 Hz exocytosis stimulation illustrating the central role of VAMP2 in evoked release. However deletion of the VAMP7 longin domain leads to a substantial TeNT-resistant response to stimulation. This, suggests that VAMP7 might itself contribute to evoked release (Hua et al. 2011) when the auto-inhibition by its LD is released (Burgo et al. 2013). In our experiments, we do not rule out the possibility that VAMP7 plays a role in the release of glutamate onto GABAergic interneurons through filopodial extensions of Mfs. It should be noted however that the properties of these excitatory synapses highly depend on the post-synaptic interneuron target, which are known to be quite diverse (Rebola, Carta, and Mulle 2017). In addition, release sites corresponding to filopodia contacts onto interneurons represent only a small minority of release sites within the stratum lucidum. In any case, our results rule out any conventional role of VAMP7 in glutamate release at a central synapse where it is abundantly expressed. This suggests that an alternate role of VAMP7 needs to be envisaged at Mf-CA3 PC synapses.

The loss of VAMP7 in mice does not cause major developmental or neurological deficits (Sato et al. 2011); (Danglot et al. 2012). VAMP7 KO mice display decreased brain weight and body temperature, increased blood glycerol, and increased anxiety (Danglot et al. 2012). In *Drosophila melanogaster*, the loss of VAMP7 results in the accumulation of autophagosomes and the block of autolysosomal degradation during basal, starvation-induced, and developmental autophagy (Takáts et al. 2013). VAMP7-deficient pancreatic β-cells show defective autophagosome formation and reduced mitochondrial function. Feeding a high-fat diet to pancreatic β-cell-specific VAMP7 KO mice exacerbated mitochondrial dysfunction, further decreased ATP production and insulin secretion, and consequently induced glucose intolerance (Aoyagi et al. 2016). In our experiments, VAMP7 KO NGF-differentiated PC12 cells were defective in the secretion of late endosomal proteins such as the tetraspanin CD63, molecules involved in autophagy such as LC3 and p62, endoplasmic reticulum proteins reticulons and atlastins and a proform of VGF (Wojnacki et al. 2020) (Filippini et al. 2023). CD82, another tetraspanin that organizes microdomains at the plasma membrane was also shown to be transported in a VAMP7-dependent manner (Danglot et al. 2010). Secretion of multivesicular late endosomes and other lysosome-related organelles further appear as a general mechanism regulated by VAMP7 in several cell types (Liu et al. 2023) (Sakamoto et al. 2024). This late endosomal autophagy-dependent secretion might allow cells to eliminate cellular elements as a complementary mechanism to degradative autophagy (Vats and Galli 2022). The neuronal molecules released by VAMP7-dependent secretion might be toxic to the donor cell as it is the case for α-synuclein (Xie et al. 2022) and peroxidated lipids and iron (Ralhan et al. 2023). In the latter case, peroxidated lipids are internalized and recycled by astrocytes (Ralhan et al. 2023). VAMP7 was shown to mediate the release of Zn^{2+} (Kukic, Kelleher, and Kiselyov 2014) but the present data could not replicate this at Mf-CA3 synapses despite a modest effect on presynaptic ZnT3 expression. These results suggest that secretion of ZnT3 might use another alternative route. VAMP7-dependent secretion was also shown to mediate the release of ATP (Fader, Aguilera, and Colombo 2012; Verderio et al. 2012). Therefore, we cannot exclude the role of VAMP7 in intercellular communication mediated by ATP and other late endosomal small molecules and peptides.

Overall, VAMP7-dependent secretion does not appear to play a direct role in the conventional synaptic release of glutamate, at least at Mf-CA3 terminals where it is particularly enriched. However, the above-mentioned data in neuronal and non-neuronal cells suggest a function related to autophagy, metabolism, and cell fitness. We cannot exclude that VAMP7 is needed at one point in the membrane remodelling of synaptic terminals, since Mf terminals are known to be very dynamic and to be at least 100 times larger in volume than conventional terminals (Rebola, Carta, and Mulle 2017). Further work is needed to test this hypothesis and to shed light on the presynaptic function of VAMP7.

Author Contributions

Bernat González i Llinares: conceptualization, investigation, writing – original draft, writing – review and editing. **Lydia Danglot:** investigation, writing – review and editing. **Thierry Galli:** conceptualization, writing – review and editing. **Christophe Mulle:** conceptualization, project administration, supervision, writing – original draft, writing – review and editing.

Acknowledgements

This work was supported by the CNRS to C.M. and by the University of Bordeaux and the Erasmus Mundus program "European Neuroscience Campus" from the Seventh Framework Programme (to B.G.L.). We would like to thank Matthijs Verhage from the Vrje University in Amsterdam for his comments on the manuscript, and Christophe Blanchet for his help with the electrophysiological analysis. We extend our gratitude to the NeurImag Imaging core facility at IPNP, Inserm U1266, Université de Paris, for their outstanding support in image acquisition and processing.

Conflicts of Interest

The authors declare no conflicts of interest.

Data Availability Statement

The raw data that support the findings of this study will be made available by the authors upon request. The data are stored on a filer (FILER3_IINS) of the CNRS laboratory, UMR 5297, following the institutional policy of the CNRS.

Peer Review

The peer review history for this article is available at https://www.webofscience.com/api/gateway/wos/peer-review/10.1111/ejn.70016.

References

Alberts, P., R. Rudge, I. Hinners, et al. 2003. "Cross Talk Between Tetanus Neurotoxin-Insensitive Vesicle-Associated Membrane Protein-Mediated Transport and L1-Mediated Adhesion." *Molecular Biology of the Cell* 14: 4207–4220. https://doi.org/10.1091/mbc.e03-03-0147.

Aoyagi, K., M. Ohara-Imaizumi, M. Itakura, et al. 2016. "VAMP7 Regulates Autophagy to Maintain Mitochondrial Homeostasis and to Control Insulin Secretion in Pancreatic β-Cells." *Diabetes* 65: 1648–1659.

Burgo, A., A. M. Casano, A. Kuster, et al. 2013. "Increased Activity of the Vesicular Soluble N-Ethylmaleimide-Sensitive Factor Attachment Protein Receptor TI-VAMP/VAMP7 by Tyrosine Phosphorylation in the Longin Domain." *Journal of Biological Chemistry* 288: 11960–11972.

Burgo, A., V. Proux-Gillardeaux, E. Sotirakis, et al. 2012. "A Molecular Network for the Transport of the TI-VAMP/VAMP7 Vesicles From Cell Center to Periphery." *Developmental Cell* 23: 166–180.

Chaineau, M., L. Danglot, and T. Galli. 2009. "Multiple Roles of the Vesicular-SNARE TI-VAMP in Post-Golgi and Endosomal Trafficking." *FEBS Letters* 583: 3817–3826.

Coco, S., G. Raposo, S. Martinez, et al. 1999. "Subcellular Localization of Tetanus Neurotoxin-Insensitive Vesicle-Associated Membrane Protein (VAMP)/VAMP7 in Neuronal Cells: Evidence for a Novel Membrane Compartment." *Journal of Neuroscience* 19: 9803–9812.

Danglot, L., and T. Galli. 2007. "What is the Function of Neuronal AP-3?" *Biology of the Cell* 99: 349–361. https://doi.org/10.1042/BC20070029.

Danglot, L., M. Chaineau, M. Dahan, et al. 2010. "Role of TI-VAMP and CD82 in EGFR Cell-Surface Dynamics and Signaling." *Journal of Cell Science* 123: 723–735.

Danglot, L., K. Zylbersztejn, M. Petkovic, et al. 2012. "Absence of TI-VAMP/Vamp7 Leads to Increased Anxiety in Mice." *Journal of Neuroscience* 32: 1962–1968.

Evstratova, A., S. Chamberland, V. Faundez, and K. Toth. 2014. "Vesicles Derived via AP-3-Dependent Recycling Contribute to Asynchronous Release and Influence Information Transfer." *Nature Communications* 5: 5516–5530.

Fader, C. M., M. O. Aguilera, and M. I. Colombo. 2012. "ATP Is Released From Autophagic Vesicles to the Extracellular Space in a VAMP7-Dependent Manner." *Autophagy* 8: 1741–1756.

Filippini, F., S. Nola, A. Zahraoui, et al. 2023. "Secretion of VGF Relies on the Interplay Between LRRK2 and Post-Golgi v-SNAREs." *Cell Reports* 42: 112221.

Filippini, F., V. Rossi, T. Galli, A. Budillon, M. D'Urso, and M. D'Esposito. 2001. "Longins: A new Evolutionary Conserved VAMP Family Sharing a Novel SNARE Domain." *Trends in Biochemical Sciences* 26: 407–409.

Galli, T., A. Zahraoui, V. V. Vaidyanathan, et al. 1998. "A Novel Tetanus Neurotoxin-Insensitive Vesicle-Associated Membrane Protein in SNARE Complexes of the Apical Plasma Membrane of Epithelial Cells." *Molecular Biology of the Cell* 9: 1437–1448.

Gordon, D. E., L. M. Bond, D. A. Sahlender, and A. A. Peden. 2010. "A Targeted siRNA Screen to Identify SNAREs Required for Constitutive Secretion in Mammalian Cells." *Traffic* 11: 1191–1204.

Gupton, S. L., and F. B. Gertler. 2010. "Integrin Signaling Switches the Cytoskeletal and Exocytic Machinery That Drives Neuritogenesis." *Developmental Cell* 18: 725–736. https://doi.org/10.1016/j.devcel.2010.02.017.

Hua, Z., S. Leal-Ortiz, S. M. Foss, et al. 2011. "V-SNARE Composition Distinguishes Synaptic Vesicle Pools." *Neuron* 71: 474–487.

Jahn, R., and R. H. Scheller. 2006. "SNAREs--engines for membrane fusion." *Nature Reviews Molecular Cell Biology* 7: 631–643.

Kaeser, P. S., and W. G. Regehr. 2014. "Molecular Mechanisms for Synchronous, Asynchronous, and Spontaneous Neurotransmitter Release." *Annual Review of Physiology* 76: 333–363.

Kukic, I., S. L. Kelleher, and K. Kiselyov. 2014. "Zn2+ Efflux Through Lysosomal Exocytosis Prevents Zn2+−Induced Toxicity." *Journal of Cell Science* 127: 3094–3103.

Lavoie, N., D. V. Jeyaraju, M. R. Peralta, L. Seress, L. Pellegrini, and K. Toth. 2011. "Vesicular Zinc Regulates the Ca2+ Sensitivity of a Subpopulation of Presynaptic Vesicles at Hippocampal Mossy fiber Terminals." *Journal of Neuroscience* 31: 18251–18265.

Liu, C., D. Liu, S. Wang, L. Gan, X. Yang, and C. Ma. 2023. "Identification of the SNARE Complex That Mediates the Fusion of Multivesicular Bodies With the Plasma Membrane in Exosome Secretion." *Journal of Extracellular Vesicles* 12: e12356.

Marchal, C., and C. Mulle. 2004. "Postnatal Maturation of Mossy Fibre Excitatory Transmission in Mouse CA3 Pyramidal Cells: A Potential Role for Kainate Receptors." *Journal of Physiology (London)* 561: 27–37.

Marneffe, C., A. Moreira-de-Sá, S. Lecomte, A. Erhardt, and C. Mulle. 2024. "Short Term Plasticity at Hippocampal Mossy fiber Synapses." *Neuroscience*. https://doi.org/10.1016/j.neuroscience.2024.09.044.

Martinez-Arca, S., R. Rudge, M. Vacca, et al. 2003. "A Dual Mechanism Controlling the Localization and Function of Exocytic v-SNAREs." *Proceedings of the National Academy of Sciences of the United States of America* 100: 9011–9016.

Muzerelle, A., P. Alberts, S. Martinez-Arca, et al. 2003. "Tetanus Neurotoxin-Insensitive Vesicle-Associated Membrane Protein Localizes to a Presynaptic Membrane Compartment in Selected Terminal Subsets of the rat Brain." *Neuroscience* 122: 59–75.

Newell-Litwa, K., S. Chintala, S. Jenkins, et al. 2010. "Hermansky-Pudlak Protein Complexes, AP-3 and BLOC-1, Differentially Regulate Presynaptic Composition in the Striatum and Hippocampus." *Journal of Neuroscience* 30: 820–831. https://doi.org/10.1523/JNEUROSCI.3400-09.2010.

Racchetti, G., A. Lorusso, C. Schulte, et al. 2010. "Rapid Neurite Outgrowth in Neurosecretory Cells and Neurons is Sustained by the Exocytosis of a Cytoplasmic Organelle, the Enlargeosome." *Journal of Cell Science* 123: 165–170. https://doi.org/10.1242/jcs.059634.

Ralhan, I., J. Chang, M. J. Moulton, et al. 2023. "Autolysosomal Exocytosis of Lipids Protect Neurons From Ferroptosis." *Journal of Cell Biology* 222, no. 6: e202207130.

Ramirez, D. M. O., and E. T. Kavalali. 2012. "The Role of non-canonical SNAREs in Synaptic Vesicle Recycling." *Cellular Logistics* 2: 20–27.

Rebola, N., M. Carta, and C. Mulle. 2017. "Operation and Plasticity of Hippocampal CA3 Circuits: Implications for Memory Encoding." *Nature Reviews. Neuroscience* 18: 208–220.

Rossi, V., D. K. Banfield, M. Vacca, et al. 2004. Longins and their Longin Domains: Regulated SNAREs and Multifunctional SNARE Regulators. *Trends in Biochemical Sciences* 29, 682–688. https//doi.org/10.1016/j.tibs.2004.10.002.

Sakamoto, M., Y. Nagata, A. Furukawa, et al. 2024. "VAMP7 Knockdown in Secretory Granules Impairs CCL2 Secretion in Mast Cells." *Biochemical and Biophysical Research Communications* 691: 149258.

Sato, M., S. Yoshimura, R. Hirai, et al. 2011. "The Role of VAMP7/TI-VAMP in Cell Polarity and Lysosomal Exocytosis in Vivo." *Traffic* 12: 1383–1393.

Scheuber, A., R. Rudge, L. Danglot, et al. 2006. "Loss of AP-3 Function Affects Spontaneous and Evoked Release at Hippocampal Mossy fiber Synapses." *Proceedings of the National Academy of Sciences of the United States of America* 103: 16562–16567.

Schoch, S., F. Deák, A. Königstorfer, et al. 2001. "SNARE Function Analyzed in Synaptobrevin/VAMP Knockout Mice." *Science* 294: 1117–1122.

Sinha, R., S. Ahmed, R. Jahn, and J. Klingauf. 2011. "Two Synaptobrevin Molecules Are Sufficient for Vesicle Fusion in Central Nervous System Synapses." *Proceedings of the National Academy of Sciences of the United States of America* 108: 14318–14323.

Söllner, T., S. W. Whiteheart, M. Brunner, et al. 1993. "SNAP Receptors Implicated in Vesicle Targeting and Fusion." *Nature* 362: 318–324.

Takamori, S., M. Holt, K. Stenius, et al. 2006. "Molecular Anatomy of a Trafficking Organelle." *Cell* 127: 831–846. https://doi.org/10.1016/j.cell.2006.10.030.

Takáts, S., P. Nagy, Á. Varga, et al. 2013. "Autophagosomal Syntaxin17-Dependent Lysosomal Degradation Maintains Neuronal Function in Drosophila." *Journal of Cell Biology* 201: 531–539.

Vats, S., and T. Galli. 2022. "Role of SNAREs in Unconventional Secretion-Focus on the VAMP7-Dependent Secretion." *Frontiers in Cell and Development Biology* 10: 884020.

Verderio, C., C. Cagnoli, M. Bergami, et al. 2012. "TI-VAMP/VAMP7 Is the SNARE of Secretory Lysosomes Contributing to ATP Secretion From Astrocytes." *Biology of the Cell* 104: 213–228.

Vergnano, A. M., N. Rebola, L. P. Savtchenko, et al. 2014. "Zinc Dynamics and Action at Excitatory Synapses." *Neuron* 82: 1101–1114.

Weber, T., B. V. Zemelman, J. A. McNew, et al. 1998. "SNAREpins: Minimal Machinery for Membrane Fusion." *Cell* 92: 759–772.

Wilhelm, B. G., S. Mandad, S. Truckenbrodt, et al. 2014. "Composition of Isolated Synaptic Boutons Reveals the Amounts of Vesicle Trafficking Proteins." *Science* 344: 1023–1028.

Wojnacki, J., S. Nola, P. Bun, et al. 2020. "Role of VAMP7-Dependent Secretion of Reticulon 3 in Neurite Growth." *Cell Reports* 33: 108536.

Xie, Y. X., N. N. Naseri, J. Fels, et al. 2022. "Lysosomal Exocytosis Releases Pathogenic α-Synuclein Species From Neurons in Synucleinopathy Models." *Nature Communications* 13: 4918.

Supporting Information

Additional supporting information can be found online in the Supporting Information section.